

Design, fabrication and optical characterizations of large-area lithography-free ultrathin multilayer selective solar coatings with excellent thermal stability in air



Hao Wang, Hassan Alshehri, Hang Su, Liping Wang*

School for Engineering of Matter, Transport & Energy, Arizona State University, Tempe, AZ 85287, USA

ARTICLE INFO

Keywords:

Solar thermal
Selective absorber
Thermal stability
Spectroscopy

ABSTRACT

A sub-micron-thick selective multilayer solar thermal absorber made of tungsten, SiO₂ and Si₃N₄ multilayer thin films was theoretically designed and experimentally demonstrated in this work. The optical performance was optimized by the particle swarm optimization algorithm for this multilayer absorber, whose spectral selectivity is associated with the Fabry-Perot resonance and anti-reflection effects. The designed multilayer absorber was deposited by sputtering and chemical vapor deposition techniques on the wafer scale. Its spectral absorptance characterized by a Fourier Transform Infrared spectrometer (FTIR) was demonstrated to be greater than 0.95 in the solar spectrum and less than 0.1 emittance in the mid-infrared with angular insensitivity. Temperature dependent FTIR measurements with an optical fiber setup revealed stable optical performance up to 600 °C in ambient, while thermal cycle testing showed its long-term thermal stability at 400 °C. Theoretical analysis of solar to power efficiency for a Carnot heat engine driven by the Solar heat was performed, which clearly shows that the proposed ultrathin selective multilayer absorber with spectral selectivity, angular insensitivity as well as high temperature stability could significantly boost the conversion efficiency of solar thermal systems at mid to high temperatures.

1. Introduction

Energy crisis in the past decades has immensely boosted the search for alternatives to traditional fossil fuels, among which solar energy stands out as an important candidate due to its cleanness and abundance. However, the relatively low conversion efficiency and energy density strongly hinder the utilization of solar energy in wider applications. Solar thermal absorber, which converts solar radiation into thermal energy, strongly affects the efficiency of energy harvest and conversion in solar thermal, solar thermoelectric and solar photovoltaic systems. Spectral selectivity is crucial for an efficient solar absorber, which is highly desired to be strongly absorbing in the visible and near-infrared (NIR) range and weakly emitting in the infrared (IR) spectral regime. In this way the collected solar energy can be maximized while the thermal emission loss from the absorber will be minimized. In addition, a consistent performance at elevated temperatures is also highly preferred for concentrating solar power (CSP) systems with a high energy density but strict requirements on the absorber's thermal stability.

Different methods have been employed to obtain selective

absorbers, including both material and structure based approaches [1]. Material based selective absorbers consist of natural or treated materials such as black paint, black chrome [2–4], Pyromark [5] as well as composites and cermet [6–11], which exhibit intrinsic selective optical properties. However, the spectral selectivity for material based selective absorbers is usually not ideal, because they exhibit high emittance in the IR. Moreover, the tunability of optical properties for the material based selective absorbers is low, making it harder to modify the optical properties to meet the requirements of different applications.

Apart from material based absorbers, spectral selectivity can be achieved in artificial materials or metamaterials constructed by micro- or nano-structures whose exotic properties cannot be found in naturally occurring materials [12]. Selective absorption peaks can be attained in metamaterials by the excitation of plasmonic resonance at particular wavelengths, which can be tuned by changing the geometric parameters of the nano-structures. Meanwhile, the transition between high visible absorptance and low IR emittance is usually sharp in metamaterials, as they usually contain metallic components which lead to highly reflective behavior beyond resonance. Various selective metamaterial absorbers have been proposed, based on gratings [13–18],

* Corresponding author.

E-mail address: liping.wang@asu.edu (L. Wang).

nanoparticles [19–21], photonic crystals [22–26], as well as cross-bar and nano-disk arrays [27,28]. However, metamaterial structures usually require complicated fabrication techniques with low throughput, making them harder to fabricate in the large scale. In addition, high temperature stability for metamaterial solar absorbers could be a concern, as it will be harder to maintain the surface topography for the nano-structures due to thermal stress caused by the high temperature.

Multilayer structures [29,30] based on the anti-reflection effect or cavity resonance were proposed as another approach to obtain selective solar absorbers, and cermet based multilayer selective absorbers [31–34] have been reported to possess a decent mid-to-high temperature stability. However, due to the possible instability induced by thermal stress and material oxidation, high temperature stability needs to be further examined for the multilayer absorbers, as well as the temperature dependent optical properties. In this work, we have theoretically designed and experimentally fabricated an ultrathin multilayer selective solar absorber. The specular reflectance was measured by an FTIR spectrometer at both near normal and oblique incidences. The hemispherical reflectance was examined by an integrating sphere coupled to a tunable light source. Moreover, the temperature dependent reflectance was measured by a novel FTIR fiber optics setup, allowing the investigation of the thermal stability for this solar absorber in ambient. Thermal cycle testing was also explored to look into the thermal stability. The multilayer sample was further characterized with a scanning electron microscope (SEM) as well as Rutherford

backscattering spectroscopy (RBS) to investigate its behavior after being heated to a high temperature in air. Theoretical analysis was also performed to evaluate the efficiency performance of the multilayer absorber.

2. Structure design and sample fabrication

2.1. Design and optimization

Fig. 1a illustrates a solar thermal power system with a Carnot heat engine driven by the high-temperature thermal energy harvested by the proposed selective multilayer solar absorber, which is made of five layers (i.e., SiO_2 - Si_3N_4 -W- SiO_2 -W from top to bottom). The thin SiO_2 and Si_3N_4 layers on the top serve as anti-reflection coatings to reduce visible light reflection and thereby enhance absorption, while the W- SiO_2 -W stack at the bottom forms a Fabry-Perot cavity [35], which exhibits enhanced absorption at its resonance wavelength within the near-infrared spectrum. Tungsten was chosen because it is a refractory metal with high melting point, making it excellent for high-temperature solar thermal absorbers, and because tungsten is highly lossy in the visible and NIR spectral regime, which enhances absorption of sunlight. In order to achieve the best performance of this selective absorber, the multiple layer thicknesses were optimized with the particle-swarm optimization (PSO) method [36,37] by maximizing the objective function defined as the solar-to-power conversion efficiency, which is calculated by:

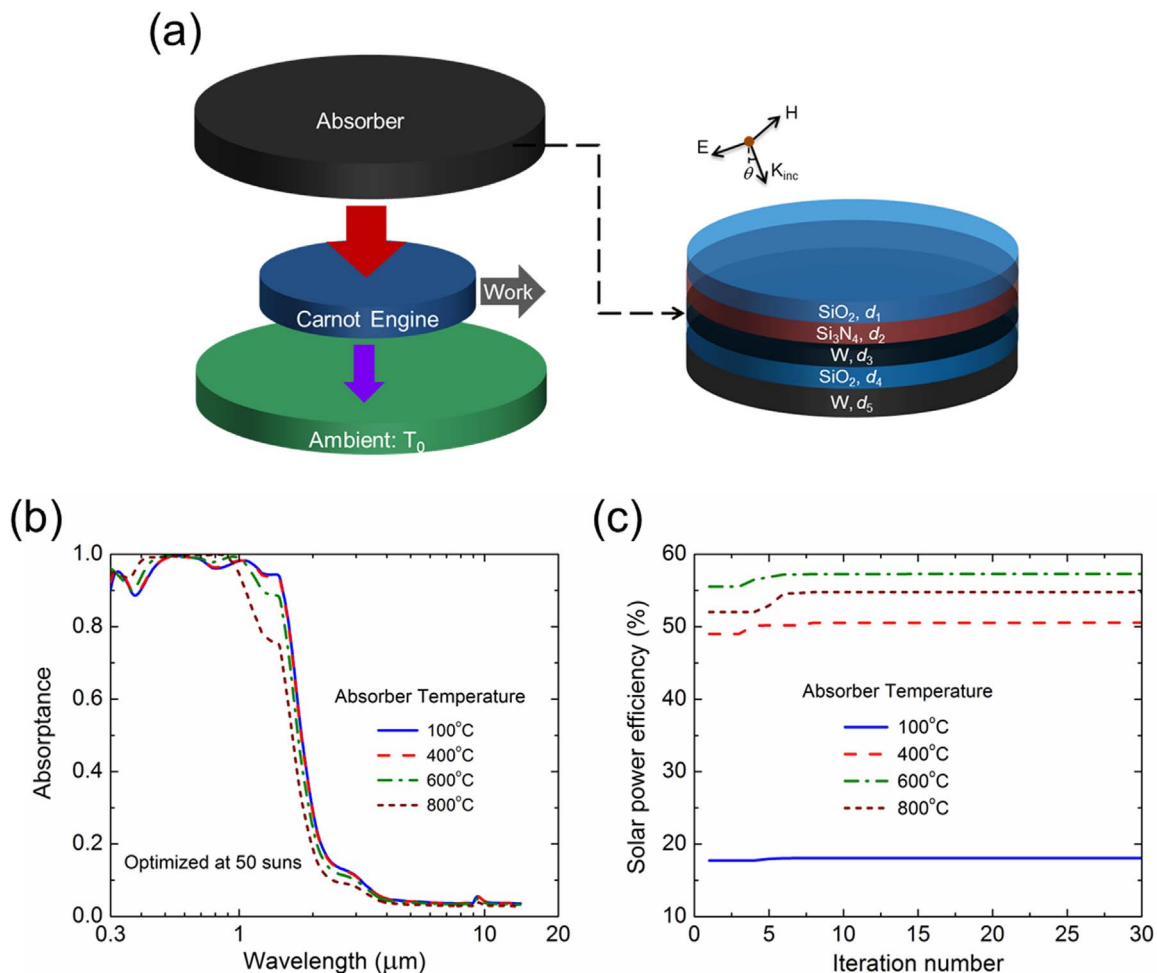


Fig. 1. (a) An illustration of a solar thermal power system with a Carnot heat engine, as well as the schematic of the proposed multilayer selective solar absorber; (b) Calculated spectral normal absorbance of optimized multilayer solar absorbers at different temperatures; (c) Calculated maximum solar-to-power efficiency with optimized multilayer solar absorbers.

$$\eta_{\text{solar-power}} = \eta_{\text{solar-thermal}} \times \eta_{\text{carnot}} = \frac{\alpha CG - \varepsilon \sigma (T_A^4 - T_0^4)}{CG} \times \left(1 - \frac{T_0}{T_A}\right) \quad (1)$$

where $\eta_{\text{solar-thermal}}$ is the solar-to-thermal efficiency, $\eta_{\text{carnot}} = 1 - T_0/T_A$ is the efficiency of a Carnot heat engine, C is the concentration factor, $G = 1000 \text{ W/m}^2$ is the total solar radiative heat flux at AM 1.5 (global tilt) [38], σ is the Stefan-Boltzmann constant, T_A is the absorber temperature, and T_0 is the environment temperature (i.e., 300 K). α and ε are respectively the total-hemispherical absorptance and emittance integrated over the entire spectral range:

$$\alpha \approx \alpha_N = \int_0^\infty \alpha'_{\lambda,N} G_{\text{AM1.5}}(\lambda) d\lambda / \int_0^\infty G_{\text{AM1.5}}(\lambda) d\lambda \quad (2)$$

$$\varepsilon \approx \varepsilon_N = \int_0^\infty \varepsilon'_{\lambda,N} I_{\text{BB}}(\lambda, T_A) d\lambda / \int_0^\infty I_{\text{BB}}(\lambda, T_A) d\lambda \quad (3)$$

where $G_{\text{AM1.5}}$ is the spectral intensity of solar radiation at AM1.5 (global tilt), $I_{\text{BB}}(\lambda, T_A)$ is the spectral blackbody radiative intensity at the solar absorber temperature of T_A , $\alpha'_{\lambda,N}$ and $\varepsilon'_{\lambda,N}$ are respectively the spectral normal absorptance and emittance of the solar absorber. According to Kirchhoff's law, $\alpha'_{\lambda,N} = \varepsilon'_{\lambda,N}$, which are to be obtained either from spectrometric measurements or theoretical modeling. Here, to simply the calculation, both α and ε are considered to be independent on the incidence angle such that $\alpha \approx \alpha_N$ and $\varepsilon \approx \varepsilon_N$, while the diffuse behavior of the multilayer selective absorber will be confirmed later by the optical characterization at oblique directions. The spectral integration range is from 0.3 to 14 μm for the calculation of α and ε due to the limited data for the optical constants obtained from Palik [39], which covers 97% energy of solar radiation and 98% energy of thermal radiation for an absorber at 1000 °C.

Fig. 1b shows the spectral absorptance for the selective solar absorber calculated with the transfer matrix method [40], with the thickness for each layer optimized with the PSO method at 50 suns (i.e., $C = 50$) and the absorber temperatures $T_A = 100 \text{ }^\circ\text{C}$, $400 \text{ }^\circ\text{C}$, $600 \text{ }^\circ\text{C}$ and $800 \text{ }^\circ\text{C}$. It is observed that after 30 iterations, the optimized solar absorbers exhibit excellent spectral selectivity with solar absorptance $\alpha > 0.95$ in the solar spectrum and thermal emittance $\varepsilon < 0.05$ in the IR range. It is also noticed that the absorption band blue shifts to shorter wavelengths for optimized absorbers at higher temperatures. This is because as the absorber temperature increases, the peak for spectral blackbody intensity will blue shift based on Wien's displacement law. Therefore, the absorption band (i.e. emission band) for the solar absorber needs to blue shift as well to suppress the total thermal emittance. Fig. 1c is the solar-to-power conversion efficiency for the optimized solar absorbers at different temperatures. It is observed that the solar-to-power efficiency with the proposed multilayer solar absorbers reaches the maxima of 18.1%, 50.6%, 57.3% and 54.8% respectively at $T_A = 100 \text{ }^\circ\text{C}$, $400 \text{ }^\circ\text{C}$, $600 \text{ }^\circ\text{C}$ and $800 \text{ }^\circ\text{C}$.

2.2. Sample fabrication

The multilayer solar absorber optimized at $T_A = 400 \text{ }^\circ\text{C}$ was selected for sample fabrication and experimental characterizations, while the targeted thicknesses for each layer along with fabrication methods and key parameters like deposition rate, chamber pressure and

Table 1

Deposition method and parameters for different layers in the proposed multilayer selective solar absorber.

Material	Deposition method	Layer thickness (nm)	Deposition rate ($\text{\AA}/\text{s}$)	Base pressure (10^{-6} Torr)	Chamber temperature ($^\circ\text{C}$)	Sputtering or RF power (W)
SiO ₂ top layer	CVD	73	~1.1	–	300	–
Si ₃ N ₄	CVD	50	~0.7	–	300	–
W thin film	RF Sputtering	10	0.4	2	–	35
SiO ₂ cavity	DC Sputtering	71	0.65	2	–	200
W substrate	DC Sputtering	200	1.2	2	–	100

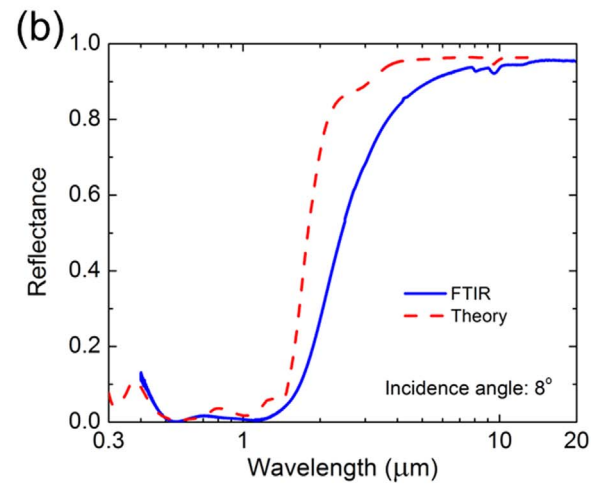
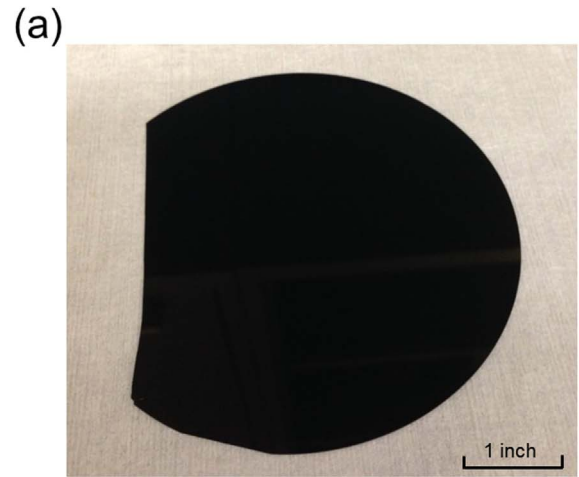


Fig. 2. (a) A photo of the fabricated multilayer selective solar absorber on a 4-in. silicon wafer; (b) Spectral directional (specular) reflectance characterized by the FTIR at an incidence angle of 8° (unpolarized).

temperature are specified in Table 1. The bottom W-SiO₂-W stack was fabricated by sputtering (Lesker PVD75 Sputter Coater), while the top thin SiO₂ and Si₃N₄ layers were deposited with chemical vapor deposition (Plasma Quest RPCVD) for better quality in order to serve as an oxygen passivation layer under heating in air. Note that the entire ultrathin multilayer stack is around 400 nm in thickness. Fig. 2(a) shows a photo for the multilayer solar absorber fabricated on a 4-in. silicon wafer, which appears black indicating its high absorptance in the visible spectral regime. Note that the multilayer absorber has zero transmission as the bottom 200-nm tungsten layer is optically opaque,

3. Results and discussion

3.1. Wavelength-selective optical and radiative properties at room temperature

The specular spectral directional reflectance R_{λ}^{sp} of the fabricated multilayer absorber was characterized by an FTIR spectrometer (Thermo Scientific, iS50) at an incidence angle of 8° with a variable-angle reflectance accessory (Harrick, Seagull) in wavelength from 0.4 to 20 μm with a resolution of 4 cm^{-1} in wavenumber. The visible and NIR reflectance (i.e., $0.4\text{ }\mu\text{m} < \lambda < 1\text{ }\mu\text{m}$) was measured by a Si detector, while a deuterated triglycine sulfate (DTGS) detector was employed for the mid-IR measurement (i.e., $1\text{ }\mu\text{m} < \lambda < 20\text{ }\mu\text{m}$). Each measurement spectrum was averaged from 32 scans with an Al mirror as the reference, and the measured reflectance was corrected by the theoretical reflectance of Al. Fig. 2b plots the specular spectral-normal reflectance measured by the FTIR as well as the theoretical reflectance for comparison. A good match between theory and measurement can be observed in the visible and NIR spectral regime, while the measured reflectance is a bit lower for $2\text{ }\mu\text{m} < \lambda < 10\text{ }\mu\text{m}$, which is most probably due to impurities during fabrication. The fabricated sample exhibits specular reflectance $R_{\lambda}^{sp} < 0.03$ within $0.5\text{ }\mu\text{m} < \lambda < 1.2\text{ }\mu\text{m}$, and $R_{\lambda}^{sp} > 0.9$ in the mid-IR at $\lambda > 5\text{ }\mu\text{m}$.

3.2. Quasi-diffuse absorption or emission from directional characterization

In addition to spectral selectivity, an ideal solar absorber should also exhibit consistent performance at various incidence angles to harvest most sunlight incident from oblique directions. In order to investigate the angular dependence of the selective multilayer solar absorber, its specular reflectance R_{λ}^{sp} was measured at oblique incidence angles with the FTIR. Note that the optical behavior may vary under different polarizations at oblique incidences. Therefore, the measurement was performed separately for transverse electric (TE) and transverse magnetic (TM) incidences. A TE wave represents an incident wave with an electric field perpendicular to the plane of incidence spanned by the incident wavevector and surface normal, while a TM wave indicates that the wave magnetic field is perpendicular to the plane of incidence. The linearly polarized incident wave was obtained using a broadband polarizer (Thorlabs, WP25M-UB) in the visible and NIR regime and the FTIR internal wire-grid polarizer in the mid-IR range.

The measured specular reflectance with oblique incidence at both TE and TM polarizations is shown in Fig. 3, for incidence angles of 5° , 15° , 30° , 45° and 60° . From Fig. 3(a) which shows the measurement for TE incidence, the reflectance barely changes at incidence angles up to 45° in the entire wavelength range, but slightly increases up to around 0.1 at the incidence angle of 60° in the visible and NIR spectral regime. On the other hand, the reflectance of this selective solar absorber barely changes in the visible and NIR range for TM incidence, but exhibits a reflection dip around $\lambda = 8\text{ }\mu\text{m}$ whose reflectance decreases down to 0.3 when the incidence angle increases up to 60° . This reflection dip is due to the Berreman leaky mode [41,42] within the phonon band of SiO_2 , where it is lossy due to the strong absorption caused by lattice vibrations. Note that the Berreman mode can only be excited for TM incidence. Overall, the spectral reflectance of the proposed multilayer sample is insensitive to the incidence angle at most wavelengths with incidence angle up to 45° for both TM and TE polarizations. In other words, the multilayer solar absorber exhibits quasi-diffuse absorption or emission behaviors.

3.3. High specularity from spectral directional-hemispherical reflectance measurements

Note that spectral directional absorptance or emittance of the multilayer solar absorber is calculated by $a_{\lambda}^i = \epsilon_{\lambda}^i = 1 - R_{\lambda}^{i\prime}$ based on energy balance, where $R_{\lambda}^{i\prime}$ is the spectral directional-hemispherical

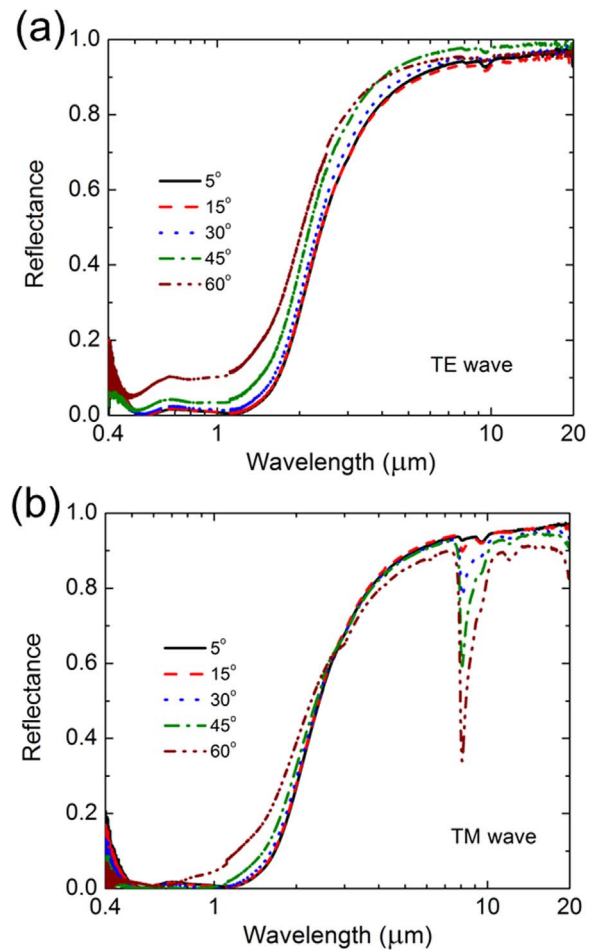


Fig. 3. Spectral directional (specular) reflectance characterized by the FTIR at various oblique incidences for (a) TE waves and (b) TM waves.

reflectance. As our FTIR reflectance accessory only measures the specular reflectance R_{λ}^{sp} , the spectral directional-hemispherical reflectance $R_{\lambda}^{i\prime}$ has to be characterized to evaluate the solar absorption and thermal emission as well as the contribution due to diffusely reflected light, especially when heated up in air. A tunable light source assembly (Newport, TLS-250QU), including a Quartz Tungsten Halogen lamp source (Newport, 6334NS), a monochromator (Newport, CS130-USB-3-FH), as well as an optical chopper (Newport, 75163) and a lock-in amplifier (Newport, Merlin), was used to perform the hemispherical and diffuse reflectance measurements. The sample was mounted at the back of an 8-in. integration sphere (Labsphere, CSTM-R/T) to measure the spectral directional-hemispherical or diffuse reflectance at an incidence angle of 8° . A light trap was employed to absorb the specular component of reflected light in order to measure the diffuse reflectance. The spectral measurement within $0.4\text{ }\mu\text{m} < \lambda < 1\text{ }\mu\text{m}$ was performed utilizing a Si detector (Thorlabs, SM05PD1A), while the measurement from $1\text{ }\mu\text{m}$ to $1.6\text{ }\mu\text{m}$ employed an InGaAs (Thorlabs, SM05PD5A) detector. An Al mirror was used as the reference and the measured reflectance was corrected based on the theoretical reflectance of Al. Both the hemispherical and diffuse reflectance was measured for the multilayer absorber sample before and after being heated at $600\text{ }^{\circ}\text{C}$ for an hour in air.

Fig. 4a shows the measurement results for the multilayer solar absorber sample before heating. It can be found that the diffuse reflectance is negligible, indicating excellent specularity of this multilayer absorber, which is expected for a planar multilayer structure without nano-structured surfaces. The hemispherical reflectance $R_{\lambda}^{i\prime}$ is also plotted for comparison with the specular reflectance R_{λ}^{sp} measured by

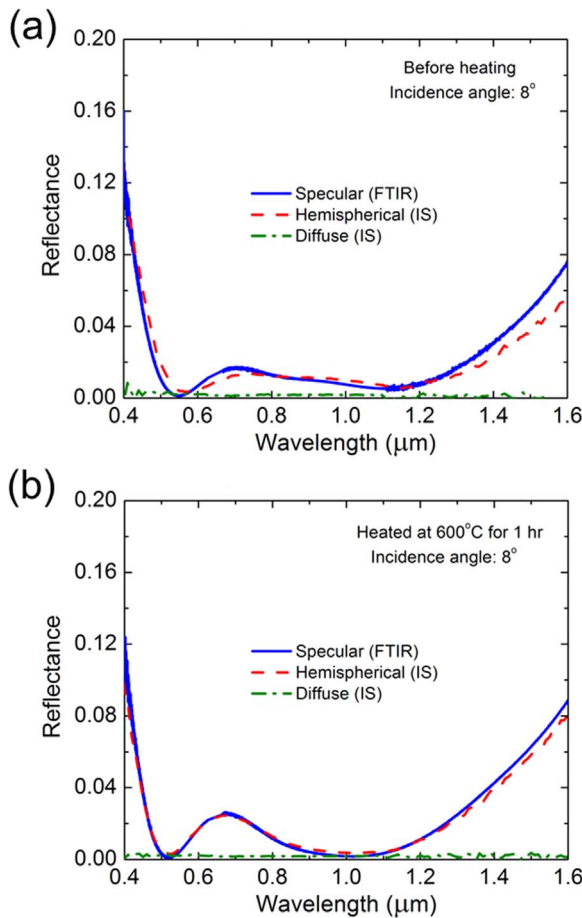


Fig. 4. Spectral directional-hemispherical and diffuse reflectance characterized by the integrating sphere for the fabricated multilayer selective absorber sample: (a) before heating; (b) after heating at 600 °C for 1 h in air.

the FTIR, which clearly proves $R_{\lambda}^{\uparrow} \approx R_{\lambda}^{sp}$ due to highly specular surface within a small difference less than 2.5%. This also suggests a good agreement between the measurement results from these two methods. As a result, the fabricated solar absorber is demonstrated to be highly absorbing in the solar spectrum while barely emitting in the mid-IR range. In addition, this sample was measured after being heated in a furnace at 600 °C for 1 h with the presence of air in order to examine its specularity after heating. It can be seen from Fig. 4b that the diffusely reflected light is still negligible after heating, demonstrating that this sample remains highly specular even after being heated at 600 °C in air for an hour. The spectral hemispherical reflectance R_{λ}^{\uparrow} of the multilayer absorber has a small change less than 3% before and after heating, indicating good thermal stability of this multilayer solar absorber.

3.4. Excellent thermal stability in air from temperature-dependent spectrometric characterization and thermal cycling test

Consistent optical performance of solar thermal absorbers at elevated temperatures is crucial, especially for CSP systems to maintain their high conversion efficiency under concentrated solar radiation. In order to study the optical and radiative properties of the multilayer solar absorber at different temperatures, a fiber optics setup coupled to the FTIR bench was employed for the temperature dependent spectral-normal reflectance measurement. An FTIR fiber coupler (Harrick, FiberMate2) was utilized to couple the signal from the FTIR internal sources into a visible–NIR (Thorlabs, RP21) or IR (High Tech Photonics, AP10757) Y-shape fiber bundle. The incident light was focused onto the sample surface via one fiber leg, and the reflected signal was collected

by the same fiber head and guided back to the FTIR detector through the other fiber leg. Meanwhile, the multilayer absorber sample was placed in a customized heater for heating in air. A thermocouple (Omega, KMTXL-040) was employed to monitor the sample temperature, while a temperature controller (Omega, CSi8D) was utilized to maintain the sample temperature at its setpoint. The sample temperature was stabilized at its setpoint for at least 30 min before each measurement. The spectral measurement was performed from 0.45 to 18 μm in wavelength, and the results were averaged from 100 scans with a resolution of 16 cm⁻¹. An Al mirror was used to measure the reference signal S_{ref} , and the sample signal S_{sample} was measured as the signal reflected from the sample surface. Note that the noise signal needs to be corrected as the fiber head will directly reflect part of the signal, which is neither reflected by the Al mirror nor the multilayer absorber sample. Therefore, the noise signal S_{noise} was measured with the optical fiber facing the ambient background. By correcting the sample reflectance with the noise signal and the theoretical reflectance of the Al mirror, the actual sample reflectance can be obtained by:

$$R_{corrected} = \frac{S_{sample} - S_{noise}}{S_{ref} - S_{noise}} \times R_{Al} \quad (4)$$

Fig. 5a shows the temperature dependent reflectance of the multilayer absorber measured by the FTIR fiber optics setup. It can be seen that the reflectance of the tested sample barely changes from room temperature to 600 °C, indicating its excellent high temperature stability. On the other hand, the visible-NIR reflectance starts to increase and the IR reflectance begins to decrease dramatically when the

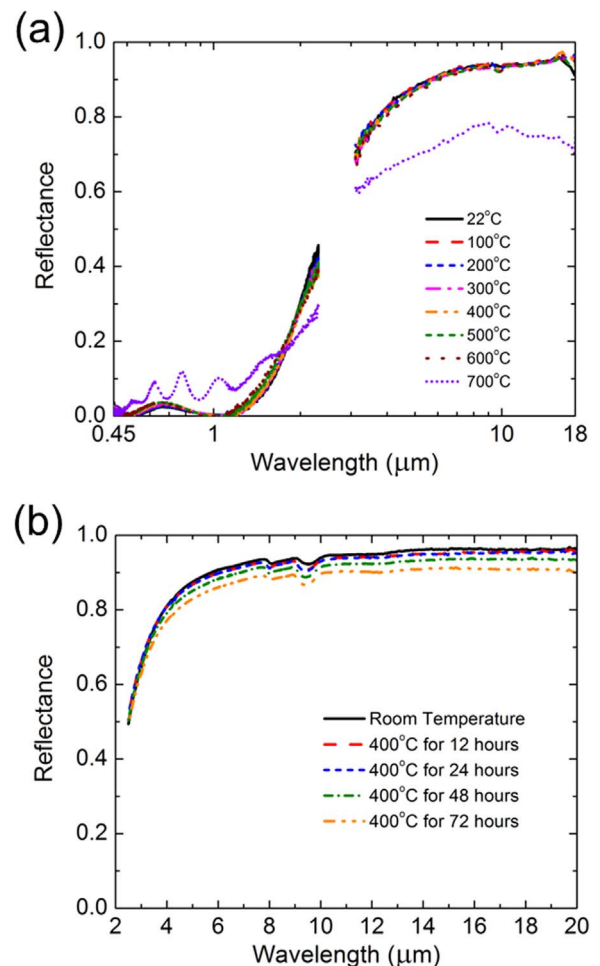


Fig. 5. (a) Temperature dependent specular reflectance characterized by FTIR fiber optics. (b) Spectral directional (specular) reflectance of the multilayer absorber measured by FTIR at room temperature after multilayer thermal cycle tests at 400 °C in air.

temperature further increases up to 700 °C. This indicates instability possibly caused by physical or chemical changes at that high temperature. Note that the spectral-normal reflectance within $2.3 \mu\text{m} < \lambda < 3.1 \mu\text{m}$, which is not covered by either the transmission band of the vis-NIR and IR optical fibers, is not shown due to the poor signal-to-noise ratio.

Although the multilayer absorber was demonstrated to possess stable performance up to 600 °C under short-term heating, it still remains a question whether it can exhibit good thermal stability in longer heating from alternating heating and cooling cycles. Therefore, a thermal cycle testing was conducted for this multilayer solar absorber sample at 400 °C in a furnace with presence of air. The multilayer absorber went through 1–6 heating/cooling cycles, while each heating/cooling cycle consists of a heating time of 12 h in furnace followed by 2 h cooling. The IR reflectance was measured after each heating/cooling cycle at room temperature as shown in Fig. 5b. It can be observed that the IR reflectance barely changes for heating within 24 h. The IR reflectance decreases a bit for longer heating but the overall absolute change of IR reflectance is within 6%.

3.5. Failure mechanisms from SEM and RBS characterizations

As indicated by Fig. 5, the optical and radiative properties of the multilayer solar absorber are stable at temperatures up to 600 °C, but degrade dramatically at 700 °C. In order to understand the reasons that cause the degradation at 700 °C, the sample was characterized under an FE-SEM (Hitachi S4700) before and after heating in air. Figs. 6a and 6b show the SEM images of the sample surface before and after being heated at 600 °C for 1 h, indicating no apparent changes. However, when the sample was further heated at 700 °C in air for 1 h, blisters with diameters around 200 μm were formed at the sample surface as shown in Fig. 6c. Possible reasons for the surface blistering could be the thermal stress due to the coefficient of thermal expansion (CTE) mismatch between the silicon wafer and the tungsten substrate, or the outgassing of helium molecules that were trapped inside the multilayer structure during the CVD process. The surface blistering could be potentially avoided by employing materials with better CTE match to reduce thermal stress or by thermal annealing to release the helium molecules.

In addition, Rutherford backscattering (RBS) analysis by impinging a helium ion beam onto the sample and measuring the back scattering condition of ions was carried out to study the chemical compositions and depth information of the multilayer selective absorber sample. Fig. 7 shows the result for the RBS analysis, where each individual peak represents the ions backscattered with a certain energy, indicating the existence of one particular element at a certain depth. It can be observed that the RBS results for the multilayer sample before and after being heated at 600 °C are almost identical, confirming its thermal stability at temperatures up to 600 °C. On the other hand, the RBS curve for the sample heated at 700 °C shows a significant difference. The peak associated with the tungsten substrate becomes lower, but expands to the lower energy region towards the bottom left. This phenomenon is due to surface blistering, as when the multilayer blisters up, part of the ions will need to penetrate a longer distance through the tungsten substrate before being scattered. Therefore, these scattered ions exhibit a lower energy due to the higher energy loss while penetrating through a longer distance in the tungsten layer. As a result, less scattered ions exhibit higher energy and the peak associated with the tungsten substrate will be lower on the high energy end. On the other hand, more scattered ions exhibit lower energy and the peak indicating the tungsten substrate will expand to a lower energy region.

3.6. Predicted solar-to-power efficiency with the multilayer selective absorber

In order to quantitatively evaluate the performance of the

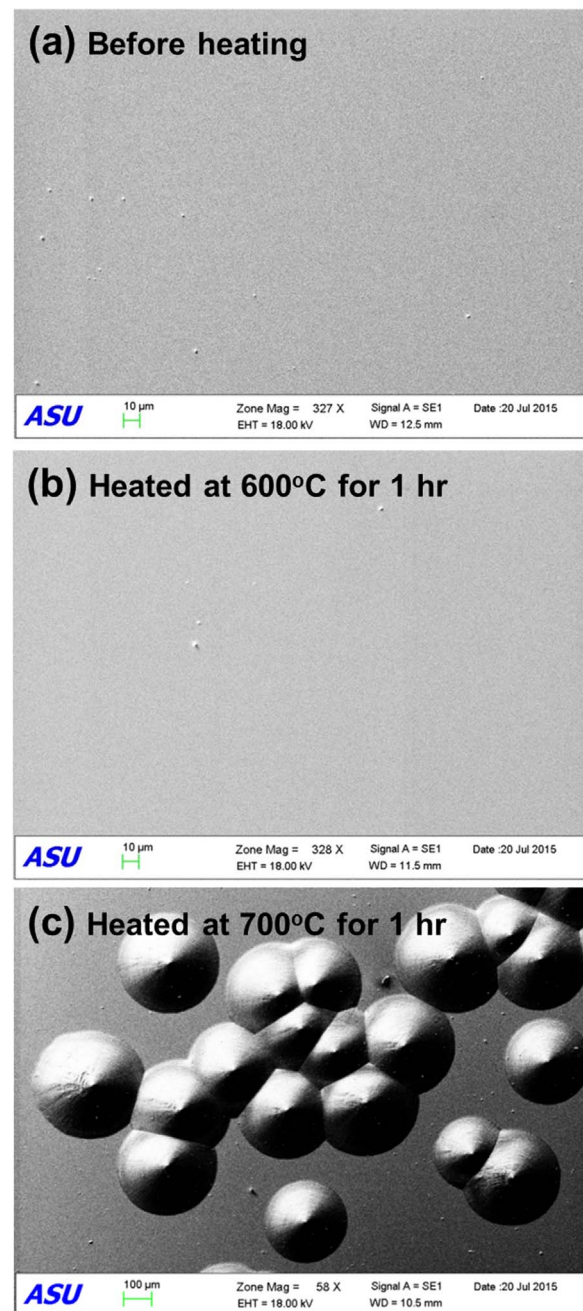


Fig. 6. SEM images of the fabricated multilayer selective solar absorber sample: (a) before heating; (b) after heated at 600 °C for 1 h in air; (c) after heating at 700 °C for 1 h in air.

multilayer selective solar absorber, its solar-to-power efficiency was theoretically investigated according to Eq. (1). Since the multilayer absorber was demonstrated to be angular-insensitive as well as thermally stable up to 600 °C, its near-normal optical and radiative properties obtained from the room temperature FTIR measurement were used for the theoretical efficiency analysis. Fig. 8a shows the solar-to-power conversion efficiency $\eta_{\text{solar-power}}$ of the ideal, multilayer, and black absorbers as the absorber temperature varies from 100 °C to 800 °C. Note that the concentration factor was fixed at $C = 5$ and the ambient temperature was considered as $T_0 = 20$ °C. An ideal absorber has an optimized cutoff wavelength, below which the spectral absorptance is unity with zero absorptance elsewhere. On the other hand, a black absorber exhibits unity absorptance or emittance over the entire wavelength range. It is observed from Fig. 8a that the $\eta_{\text{solar-power}}$ for the

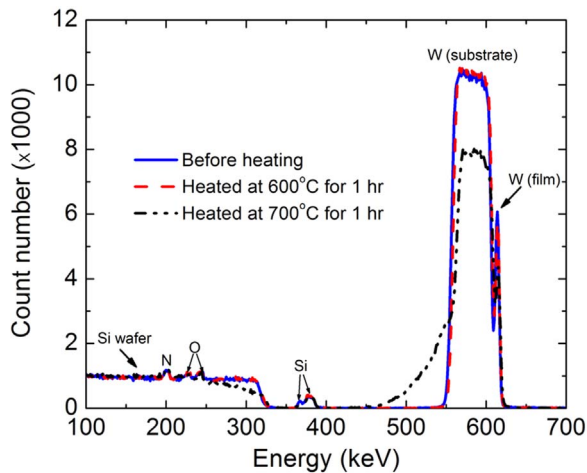


Fig. 7. RBS characterization results of the fabricated multilayer selective solar absorber sample before and after heating at 600 °C or 700 °C for 1 h in air.

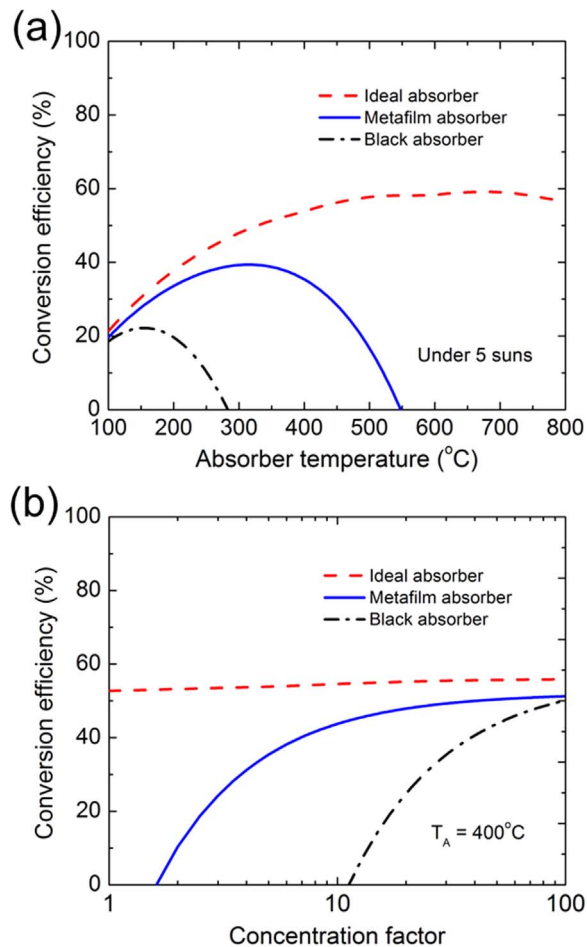


Fig. 8. Theoretical solar-to-power efficiencies for the ideal selective absorber, the fabricated multilayer selective absorber, and the black absorber when coupled with a Carnot heat engine at: (a) different absorber temperatures with a fixed concentration factor of 5; (b) varied concentration factors with a fixed absorber temperature of 400 °C.

three absorbers are comparable at low absorber temperature $T_A = 100$ °C: 21.3% for the ideal absorber, 19.6% for the multilayer absorber, and 18.5% for the black absorber, respectively. There is expected because the thermal re-emission loss is negligible when the absorber temperature is low, hence spectral selectivity to minimize the thermal re-emission loss does not have a noticeable impact on the performance

of the absorber. On the other hand, the three different absorbers show remarkably different performances when the absorber temperature becomes higher. It is found that the highest solar-to-power efficiency for the ideal, multilayer and black absorber are respectively 59.1%, 39.4% and 22.1% but at different absorber temperatures. The conversion efficiency of the multilayer absorber drops to zero at a temperature of 550 °C, or called stagnation temperature where no solar energy is converted to power. On the other hand, the stagnation temperature for the black absorber is much lower at 280 °C. Nevertheless, the conversion efficiency of the ideal absorber is still as high as 56% when the temperature reaches 800 °C. This demonstrates the importance of spectral selectivity in improving the performance of solar thermal absorbers at high temperatures.

Fig. 8b shows the solar-to-power conversion efficiency for the three types of absorber when the concentration factor varies from 1 to 100 at the fixed absorber temperature $T_A = 400$ °C. It can be observed that the solar-to-power conversion efficiency increases with a higher concentration factor, since the energy loss through thermal re-emission will be relatively smaller when compared with a larger input solar radiation. It is also found that the difference between the efficiency of the three absorbers is large at smaller concentration factors, but becomes less significant as the concentration factor increases. This is because spectral selectivity is less important at larger concentration factors when the thermal re-emission loss becomes negligible. The multilayer absorber could convert 40% of solar radiation into power under 5 suns, 42% under 10 suns, and 51% under 100 suns, but none when the concentration is below 1.6 suns. In comparison, at least of 10.5 suns concentration is required for the black absorber to obtain nonzero power from sunlight.

4. Conclusions

In this work, a multilayer selective solar absorber made of SiO_2 - Si_3N_4 - W - SiO_2 - W stacks was theoretically designed, experimentally fabricated, and optically characterized. FTIR measurements indicate excellent spectral selectivity from this multilayer absorber with solar absorptance larger than 0.95 in the visible and near IR, as well as emittance less than 0.1 in the IR spectral regime. Oblique reflectance was also characterized by the FTIR for both TE and TM polarizations, demonstrating its insensitivity to incidence angles. On the other hand, the diffuse reflectance was measured in the integrating sphere coupled with a tunable light source, indicating high specularity of this multilayer absorber both before and after being heated at 600 °C. In addition, high temperature stability was investigated by the temperature dependent reflectance measurement with FTIR fiber optics, proving its excellent thermal stability up to 600 °C in air. Thermal cycling test revealed that the developed multilayer selective absorber is thermally stable at 400 °C for up to 72 h heating in air. In order to investigate the causes for the thermal degradation above 600 °C, the sample was characterized by both SEM and RBS techniques after being heated at 700 °C, where surface blistering is observed to be responsible for the change of optical properties at higher temperatures. The surface blistering, which is possibly due to CTE mismatch or outgassing from the structure, could be further avoided by better material selection and fabrication procedures for possible better thermal stability above 600 °C. Theoretical efficiency analysis was also performed for the developed multilayer selective absorber, indicating its overwhelming conversion efficiency compared with a black surface, while there is still room for improvement to approach to the performance of the ideal absorber. The insights gained from this work will facilitate the research and development of novel selective solar thermal absorbers with excellent spectral selectivity and thermal stability at high temperatures to boost the performances in various solar thermal power systems.

Acknowledgements

This work was mainly supported by the National Science Foundation under Grant number CBET-1454698 (L.W.) and the US-Australia Solar Energy Collaboration - Micro Urban Solar Integrated Concentrators (MUSIC) project sponsored by the Australian Renewable Energy Agency (H.W.). H.A. would like to thank King Saud University and the Saudi Arabian Cultural Mission (SACM) for their sponsorship for his Ph.D. study at ASU. We would like to thank ASU Center for Solid State Electronics Research to provide cleanroom facility for sample fabrication and ASU LeRoy Eyring Center for Solid State Science to use the Ion Beam Analysis of Materials facility for the SEM and RBS characterizations.

References

- [1] I.E. Khodasevych, L. Wang, A. Mitchell, G. Rosengarten, Micro and nanostructured surfaces for selective solar absorption, *Adv. Opt. Mater.* 3 (2015) 852–881.
- [2] R. Pettit, R. Sowell, I. Hall, Black chrome solar selective coatings optimized for high temperature applications, *Sol. Energy Mater.* 7 (1982) 153–170.
- [3] G.E. McDonald, Spectral reflectance properties of black chrome for use as a solar selective coating, *Sol. Energy* 17 (1975) 119–122.
- [4] J. Sweet, R. Pettit, M. Chamberlain, Optical modeling and aging characteristics of thermally stable black chrome solar selective coatings, *Sol. Energy Mater.* 10 (1984) 251–286.
- [5] C.K. Ho, A.R. Mahoney, A. Ambrosini, M. Bencomo, A. Hall, T.N. Lambert, Characterization of Pyromark 2500 paint for high-temperature solar receivers, *J. Sol. Energy Eng.* 136 (2014) 014502.
- [6] D. Ding, W. Cai, Self-assembled nanostructured composites for solar absorber, *Mater. Lett.* 93 (2013) 269–271.
- [7] L. Gaouyat, Z. He, J.-F. Colomer, P. Lambin, F. Mirabella, D. Schryvers, O. Deparis, Revealing the innermost nanostructure of sputtered NiCo X solar absorber cermet, *Sol. Energy Mater. Sol. Cells* 122 (2014) 303–308.
- [8] E. Wäckelgård, A. Mattsson, R. Bartali, R. Gerosa, G. Gottardi, F. Gustavsson, N. Laidani, V. Micheli, D. Primetzhofer, B. Rivolta, Development of W–SiO₂ and Nb–TiO₂ solar absorber coatings for combined heat and power systems at intermediate operation temperatures, *Sol. Energy Mater. Sol. Cells* 133 (2015) 180–193.
- [9] J. Cheng, C. Wang, W. Wang, X. Du, Y. Liu, Y. Xue, T. Wang, B. Chen, Improvement of thermal stability in the solar selective absorbing Mo–Al₂O₃ coating, *Sol. Energy Mater. Sol. Cells* 109 (2013) 204–208.
- [10] Q.-C. Zhang, Stainless-steel–AlN cermet selective surfaces deposited by direct current magnetron sputtering technology, *Sol. Energy Mater. Sol. Cells* 52 (1998) 95–106.
- [11] L. Tang, F. Cao, Y. Li, J. Bao, Z. Ren, High performance mid-temperature selective absorber based on titanium oxides cermet deposited by direct current reactive sputtering of a single titanium target, *J. Appl. Phys.* 119 (2016) 045102.
- [12] Y. Liu, X. Zhang, Metamaterials: a new frontier of science and technology, *Chem. Soc. Rev.* 40 (2011) 2494–2507.
- [13] H. Wang, L. Wang, Perfect selective metamaterial solar absorbers, *Opt. Express* 21 (2013) A1078–A1093.
- [14] L. Wang, Z. Zhang, Wavelength-selective and diffuse emitter enhanced by magnetic polaritons for thermophotovoltaics, *Appl. Phys. Lett.* 100 (2012) 063902.
- [15] H. Wang, V.P. Sivan, A. Mitchell, G. Rosengarten, P. Phelan, L. Wang, Highly efficient selective metamaterial absorber for high-temperature solar thermal energy harvesting, *Sol. Energy Mater. Sol. Cells* 137 (2015) 235–242.
- [16] B.J. Lee, Y.-B. Chen, S. Han, F.-C. Chiu, H.J. Lee, Wavelength-selective solar thermal absorber with two-dimensional nickel gratings, *J. Heat Transf.* 136 (2014) 072702.
- [17] S. Han, J.H. Shin, P.H. Jung, H. Lee, B.J. Lee, Broadband solar thermal absorber based on optical metamaterials for high temperature applications, *Adv. Opt. Mater.* 4 (2016) 1265–1273.
- [18] W. Wang, Y. Qu, K. Du, S. Bai, J. Tian, M. Pan, H. Ye, M. Qiu, Q. Li, Broadband optical absorption based on single-sized metal-dielectric-metal plasmonic nanostructures with high- ϵ metals, *Appl. Phys. Lett.* 110 (2017) 101101.
- [19] J. Dai, F. Ye, Y. Chen, M. Muhammed, M. Qiu, M. Yan, Light absorber based on nano-spheres on a substrate reflector, *Opt. Express* 21 (2013) 6697–6706.
- [20] M. Yan, J. Dai, M. Qiu, Lithography-free broadband visible light absorber based on a mono-layer of gold nanoparticles, *J. Opt.* 16 (2014) 025002.
- [21] H. Wang, K. O’dea, L. Wang, Selective absorption of visible light in film-coupled nanoparticles by exciting magnetic resonance, *Opt. Lett.* 39 (2014) 1457–1460.
- [22] V. Stelmakh, Y. Rinnerbauer, S. Ndao, Y.X. Yeng, J.J. Senkevich, K.F. Jensen, J.D. Joannopoulos, M. Soljačić, I. Celanovic, High-temperature tantalum tungsten alloy photonic crystals: stability, optical Properties, and fabrication, *Appl. Phys. Lett.* 103 (2013) 123903.
- [23] I. Celanovic, N. Jovanovic, J. Kassakian, Two-dimensional tungsten photonic crystals as selective thermal emitters, *Appl. Phys. Lett.* 92 (2008) 193101.
- [24] V. Rinnerbauer, S. Ndao, Y.X. Yeng, J.J. Senkevich, K.F. Jensen, J.D. Joannopoulos, M. Soljačić, I. Celanovic, R.D. Geil, Large-area fabrication of high aspect ratio tantalum photonic crystals for high-temperature selective emitters, *J. Vac. Sci. Technol. B* 31 (2013) 011802.
- [25] P. Li, B. Liu, Y. Ni, K.-K. Liew, J. Sze, S. Chen, S. Shen, Large-scale nanophotonic solar selective absorbers for high-efficiency solar thermal energy conversion, *Adv. Mater.* 27 (2015) 4585–4591.
- [26] D. Jiang, W. Yang, A. Tang, A refractory selective solar absorber for high performance thermochemical steam reforming, *Appl. Energy* 170 (2016) 286–292.
- [27] M.G. Nielsen, A. Pors, O. Albrektsen, S.I. Bozhevolnyi, Efficient absorption of visible radiation by gap plasmon resonators, *Opt. Express* 20 (2012) 13311–13319.
- [28] K. Chen, R. Adato, H. Altug, Dual-band perfect absorber for multispectral plasmon-enhanced infrared spectroscopy, *ACS Nano* 6 (2012) 7998–8006.
- [29] M. Langlais, H. Bru, P. Ben-Abdallah, High temperature layered absorber for thermo-solar systems, *J. Quant. Spectrosc. Radiat. Transf.* 149 (2014) 8–15.
- [30] Z. Nuru, M. Msimanga, C. Arendse, M. Maaza, Heavy ion elastic recoil detection analysis of Al_xO_y/Pt/Al_xO_y multilayer selective solar absorber, *Appl. Surf. Sci.* 298 (2014) 176–181.
- [31] A. Soum-Glaude, A. Le Gal, M. Bichotte, C. Escape, L. Dubost, Optical characterization of TiAlN_x/TiAlN_y/Al₂O₃ tandem solar selective absorber coatings, *Sol. Energy Mater. Sol. Cells* 170 (2017) 254–262.
- [32] A. Dan, J. Jyothi, K. Chattopadhyay, H.C. Barshilia, B. Basu, Spectrally selective absorber coating of WAlN/WAlON/Al₂O₃ for solar thermal applications, *Sol. Energy Mater. Sol. Cells* 157 (2016) 716–726.
- [33] A. Dan, K. Chattopadhyay, H.C. Barshilia, B. Basu, Thermal stability of WAlN/WAlON/Al₂O₃ based solar selective absorber coating, *MRS Adv.* 1 (2016) 2807–2813.
- [34] H. Liu, T. Fu, M. Duan, Q. Wan, Y. Chen, D. Fu, F. Ren, Q. Li, X. Cheng, B. Yang, Structure and thermal stability of spectrally selective absorber based on AlCrON coating for solar-thermal conversion applications, *Sol. Energy Mater. Sol. Cells* 157 (2016) 108–116.
- [35] L. Wang, S. Basu, Z. Zhang, Direct measurement of thermal emission from a Fabry–Perot cavity resonator, *J. Heat Transf.* 134 (2012) 072701.
- [36] J. Robinson, Y. Rahmat-Samii, Particle swarm optimization in electromagnetics, *IEEE Trans. Antenn. Prop.* 52 (2004) 397–407.
- [37] N. Jin, Y. Rahmat-Samii, Advances in particle swarm optimization for antenna designs: real-number, binary, single-objective and multiobjective implementations, *IEEE Trans. Antenn. Prop.* 55 (2007) 556–567.
- [38] Air Mass 1.5 Spectra, American Society for Testing and Materials (ASTM), Available from: <<http://rredc.nrel.gov/solar/spectra/am1.5/>>.
- [39] E.D. Palik, Handbook of Optical Constants of Solids, Academic press, San Diego, CA, 1998.
- [40] Z.M. Zhang, Nano/microscale Heat Transfer, McGraw-Hill, New York, 2007.
- [41] S. Vasant, J.-P. Hugonin, F. Marquier, J.-J. Greffet, Berreman mode and epsilon near zero mode, *Opt. Express* 20 (2012) 23971–23977.
- [42] Y.-B. Chen, F.-C. Chiu, Trapping mid-infrared rays in a lossy film with the Berreman mode, epsilon near zero mode, and magnetic polaritons, *Opt. Express* 21 (2013) 20771–20785.